Global and Planetary Change 208 (2022) 103687

Contents lists available at ScienceDirect

Global and Planetary Change

journal homepage: www.elsevier.com/locate/gloplacha

Meteorological causes of the catastrophic rains of October/November 2019 in equatorial Africa

Sharon E. Nicholson [a,*], Andreas H. Fink [b], Chris Funk [c], Douglas A. Klotter [a], Athul Rasheeda Satheesh [b]

[a] Earth, Ocean and Atmospheric Science, Florida State University, Tallahassee, FL, United States of America
[b] Karlsruhe Institute of Technology, Karlsruhe, Germany
[c] Climate Hazards Center, UC Santa Barbara, Santa Barbara, CA, United States of America

ARTICLE INFO

Editor: Howard Falcon-Lang

Keywords:
Climate extremes
Equatorial Africa
Eastern Africa
Global climate change

ABSTRACT

The rains of October and November 2019 brought disaster to much of equatorial Africa. In East Africa tremendous rains triggered flooding and landslides in Kenya, causing over 100 deaths and the displacement of some 18,000 people. The situation was exacerbated by an unprecedented locust plague made possible by the intense rains. Floods in the Democratic Republic of the Congo displaced some 40,000 people. The level of the Mono River jumped a meter in four days, producing floods that affected some 50,000 residents of Benin and Togo.

This article places the October and November 2019 rainfall extremes in historic context and analyzes the juxtaposition of forcings required to explain these unprecedented hydro-climatic extremes in equatorial Africa. The meteorological factors considered include the Dipole Mode Index, zonal winds over the central Indian Ocean, the Walker circulation, moisture flux and divergence, ENSO and tropical sea-surface temperatures in the Atlantic and Indian Oceans, and zonal circulation.

The Dipole Mode Index reached record levels and anomalously high values persisted for five months. This was clearly a major factor in eastern Africa. The impact there was enhanced by increased moisture flux from the Indian Ocean and a marked reduction of the descending branch of the Indian Ocean Walker cell, which strongly controls October–November rainfall. The factors in other regions included extremely warm SSTs in the tropical eastern Atlantic Ocean, the Walker circulation, anomalous moisture flux and flux divergence, and changes in the zonal winds.

1. Introduction

The rains of October and November 2019 brought disaster to much of equatorial Africa (Mekonnen, 2020; Wainwright et al., 2020). The event appears to be unprecedented, bringing forth the specter of possible climate change in equatorial Africa. Notably, climate models predict such a change under global warming (Wainwright et al., 2020, 2021). In October in Kenya and other regions of eastern Africa, tremendous rains triggered flooding and landslides, causing over 100 deaths and displacing of some 18,000 people (http://floodlist.com/africa/kenya-floods-november-2019). Lake Victoria rose over one meter within months. The severity of the situation was exacerbated by, and exacerbated, an unprecedented locust plague resulting from the intense rains (http://www.fao.org/ag/locusts/en/info/info/index.html). In Uganda, Kenya, Ethiopia, and Somalia, this was the worst outbreak in 70 years. There the locust outbreak reduced food security in a region where nearly 25 million people were already acutely food-insecure (Koros, 2020, https://www.unocha.org/east-africa-locust-infestation). Extreme rainfall also occurred in southeastern Ethiopia and equatorial regions far to the west of eastern Africa. Floods in the Democratic Republic of the Congo (DRC) affected some 60,000 people (http://floodlist.com/africa/democratic-republic-congo-ubangi-river-floods-november-2019). In October the level of the Mono River jumped nearly a meter in four days, producing floods that affected some 50,000 residents of Benin and Togo (http://floodlist.com/africa/togo-benin-moro-river-floods-october).
These conditions, combined with COVID-19, conflict and widespread extreme rains during the following 2020 March–May rainy season, have pushed equatorial Africa into a severe food crisis. According to May

* Corresponding author.
E-mail address: snicholson@fsu.edu (S.E. Nicholson).

https://doi.org/10.1016/j.gloplacha.2021.103687
Received 25 February 2021; Received in revised form 16 July 2021; Accepted 25 October 2021
Available online 30 October 2021

assessments by the Famine Early Warning Systems Network (FEWS-NET) 7.5–9 million people in Nigeria, DRC, South Sudan, and Ethiopia and 5–7.5 people in Kenya, Sudan and Somalia face extreme levels of hunger and are in desperate need of humanitarian assistance (https://fews.net/sites/default/files/Food_Assistance_Peak_Needs_April2020.pdf).

Media coverage of these events has been extensive and the Kenyan Meteorological Department has tentatively attributed the disastrous conditions in eastern Africa to the Indian Ocean Dipole (IOD). While numerous studies have demonstrated the influence of the Indian Ocean Dipole in the interannual variability of the October–November rains in this region (e.g., Webster et al., 1999; Slingo et al., 2005; Behera et al., 2005; Bahaga et al., 2019), the forcing mechanisms controlling the East African October–November rains are considerably more complicated (see Section 5). There are strong links also to El Niño-Southern Oscillation (ENSO) (Anyah and Semazzi, 2006) and to zonal winds over the central equatorial Indian Ocean (Hastenrath, 2007; Hastenrath et al., 2011), which can operate independent from the IOD (Nicholson, 2015). Moreover, the IOD has not been implicated as an important factor in many other areas affected by the flooding, notably the Guinea Coast (e.g., Nicholson et al., 2018a). Hence the totality of the October–November extremes probably resulted from the juxtaposition of several partially interrelated factors.

The extreme 2019 precipitation events arise in a warming world, in which we anticipate more extreme precipitation events, and recent disaster statistics identify the high global costs associated with such disasters (Funk, 2021), more than 79 billion dollars between 2015 and 2018.

Human induced warming can modify both the dynamic and thermodynamic properties of the climate system (Emori and Brown, 2005). 'Thermodynamic' changes are associated with a warmer atmosphere's increased specific humidity (Trenberth et al., 2003). While model simulations tend to follow thermodynamic constraints, observational results are more mixed (Muller and Takayab, 2020). In Africa, where data support is limited, there does appears to be robust evidence for increases in wet extremes, especially in wet areas (Harrison et al., 2019). In addition to thermodynamic controls, which perpetuate via changes in air temperatures, it has been argued that exceptionally warm tropical sea surface temperatures, such as those associated with the IOD, will become more extreme due to climate change (Cai et al., 2013, 2014). The 2019 event was characterized by cooler SSTs near Sumatra-Java, a pattern anticipated in the current generation of climate change simulations (Wang et al., 2020). If climate change brings more hydroclimatic extremes to equatorial Africa, then a key aspect of anticipating, predicting and responding to these hazards will be an enhanced understanding of how they occur. This study pursues such enhanced comprehension.

Fig. 1 provides an overview of the Climate Hazards Infrared Precipitation with Stations Version 2 (CHIRPS2) (Funk et al., 2015) anomalies for October and November of 2019 and compares them with the long-term mean (LTM) for the period 1981 to 2010. What is notable about the anomalies is not only their magnitude but also their exceptionally large spatial extent. While the media has emphasized the situation in eastern Africa, the anomalous rainfall extended well beyond there. During October positive anomalies were nearly ubiquitous throughout equatorial Africa, in the latitudinal span between 15° N and 10°-15° S. The few exceptions are mainly in the Congo Basin and over the Guinea highlands in the west. Pan-equatorial rainfall anomalies of the same sign during the boreal autumn are quite unusual (Nicholson, 1986a, 1986b; Nicholson, 2014). In October, rainfall was more than 400% above normal in eastern Kenya and the northern-most Sahel. In November, positive anomalies were less extensive in equatorial regions overall but more extensive in eastern Africa. Rainfall was 150–400% above normal over most of eastern Africa and along the Guinea Coast of West Africa and more than 400% above normal in northern Somalia.

This article places these rainfall extremes into historic context and

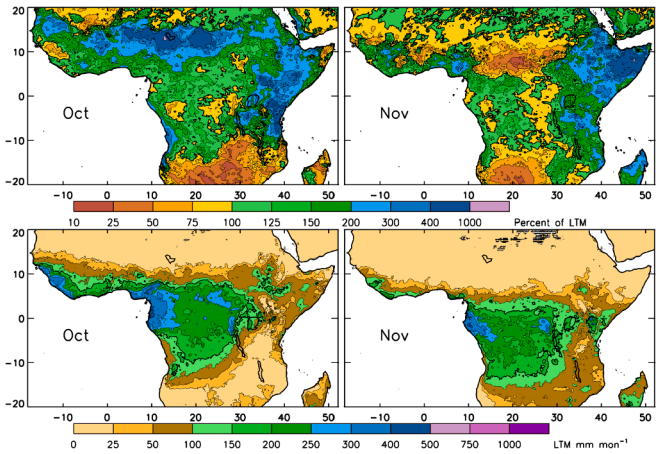

Fig. 1. Percent of long-term mean (LTM) rainfall for October (top left) and November (top right) and LTM for October (bottom left) and November (bottom right). The long-term mean is based on the years 1981–2010.

analyzes the justaposition of forcings suggested to explain these unprecedented hydro-climatic extremes in equatorial Africa. Note, however that in East Africa, strong rainfall anomalies persisted past the end of the East African long rains into January 2020 (Wainwright et al., 2020). Satellite rainfall estimates are compared with a large number of available gauge records (Sections 3 and 4). The meteorological analysis is limited to October and November 2019, the months of highest rainfall anomalies. This is the heart of the "short rains" in eastern Africa, the end of the Sahelian monsoon season and secondary rainy season along the Guinea Coast, and the peak rainy season in much of central and western equatorial Africa. It is well known that the interannual variability in these regions is governed by different factors. In order to get a more in-depth picture of forcing factors, these five regions of equatorial Africa (Fig. 2) are discussed independently in the results section.

The meteorological factors examined in this study include the Dipole Mode Index (DMI) (a widely used index to describe the state of the IOD), zonal winds, the Walker circulation over Africa and the Indian Ocean, moisture flux and divergence fields, tropical sea-surface temperatures (SSTs) in the Atlantic and Indian Oceans, and tropical waves, namely the Madden-Julian Oscillation, Kelvin, and African easterly waves (AEWs). The results are presented in Section 5. Summary and conclusions concerning operative factors are presented in Section 6.

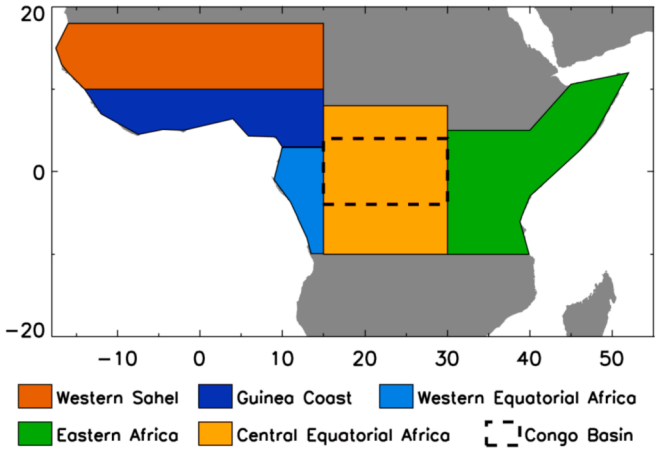

Fig. 2. Location of Sahel, Guinea Coast, western equatorial Africa, central equatorial Africa, and eastern Africa.

2. Data

Both satellite-gauge and gauge estimates of precipitation data are evaluated. Two gauge-calibrated satellite products are used: the CHIRPS version 2 satellite-gauge product (Funk et al., 2015) and the Integrated Multi satellitE Retrievals for Global Precipitation Measurement (GPM) mission (IMERG) V6 final product (Huffman et al., 2020). CHIRPS2 has a daily temporal resolution and a spatial resolution of 0.05° and is available from 1981 through present. CHIRPS2 has been validated over several areas of equatorial and West Africa and has shown excellent agreement with gauge data (Kimani et al., 2017, 2018; Cattani et al., 2018; Dinku et al., 2018; Nicholson et al., 2019; Satge et al., 2020).

While it has a long period of record, the CHIRPS archive is limited in its use of satellite information. To achieve a 40-year period of record, it relies solely on geostationary thermal infrared (TIR) satellite observations, which prior to ~2001 lack the temporal resolution to resolve sub-daily precipitation variations. However, because of the extensive validation, it is used to assess monthly rainfall. The IMERG product, on the other hand, uses half-hourly TIR observations, Passive Microwave, and the dedicated GPM Core Observatory satellite (Skofronick-Jackson et al., 2017) to produce 0.1° 2000-present half-hourly precipitation estimates. In this study, the original GPM IMERG product was remapped to 1°x1° lat./lon. and six-hourly resolution. While the CHIRPS product provides a deeper historical context, the IMERG likely provides a more physically-based representation of precipitation, because it uses passive microwave and GPM Core Observatory retrievals, which unlike TIR observations, have the capacity to detect hydrometeors, not just cloud tops. Because of its higher temporal resolution, IMERG is used in the analysis of Kelvin waves. The CHIRPS dataset, which has a longer period of record and more African station observations, is used to place the October and November precipitation extremes in historical context.

Gauge records are also considered because, being point sources, they provide direct and more accurate measurements of rainfall. Miscellaneous gauge data for October and November 2019 were obtained from the Worldwide Climate Data website of the German Weather Service (https://www.dwd.de/DE/leistungen/klimadatenweltweit/klimadatenweltweit.html). This was supplemented with information provided by additional meteorological services in Africa. Data for Angola and Zambia were obtained from the SASSCAL Weathernet website (sasscalweathernet.org). Overall, monthly totals for some 338 stations in equatorial Africa were available for October–November 2019, many more than are usually available from publicly available sources such as the Global Telecommunication System of the World Meteorological Organization.

The NIC131 gauge data set (Nicholson et al., 2018b) is also used to establish connections between rainfall in the five regions evaluated and the potential forcing factors examined, using linear correlation. The time period 1981 to 2010 is considered. The first year corresponds to the first year of CHIRPS2 data and the last year is the last with extensive data in some of the equatorial regions.

Calculations of atmospheric circulation variables (winds, divergence, streamlines, moisture divergence and flux) are based on the ERA5 reanalysis, which commences in 1979 (Hersbach et al., 2020). ERA5 provides hourly coverage at roughly 31 km global resolution on 137 vertical levels.

Sea surface temperature (SST) anomalies are obtained from the NOAA Extended Reconstructed V5 (ERST.v5) data set (Woodruff et al., 2011). The value of the DMI is calculated from that data set as well. The DMI is calculated as the difference between SST anomalies in an eastern (90°E-110°E,10°S-0°S) and a western sector (60°E-80°E,10°S-10°N) of the central Indian Ocean. Fig. 2 shows those sectors, as well as other geographical regions referred to in this work. The labels serve simply to facilitate discussion and are not strictly correct geographically speaking. These include eastern Africa, the western Sahel, central equatorial Africa (primarily the Congo Basin), western equatorial Africa (primarily the Republic of the Congo and Gabon), and the Guinea Coast.

Anomalies are calculated with respect to a 30-year period, which is standard. Since CHIRPS2 does not begin until 1981, the long-term mean used in each analysis is for the period 1981–2010. References are made to numerous countries, which are shown in Supplementary Fig. 1.

3. Rainfall in October 2019

3.1. Eastern Africa

Fig. 3 shows October rainfall totals at gauges as point data, as totals from CHIRPS2, and as the difference between CHIRPS2 and the long-term average. Country names are provided in Supplementary Fig. 1. Overall there is good agreement between CHIRPS and gauge data, even on a relatively small scale. For example, both gauges and satellite capture the drier conditions in northwest and central Kenya and the maxima to the north of Lake Victoria and in south Central Kenya. However, in October CHIRPS2 appeared to underestimate rainfall over Uganda and much of Kenya. There and in southern Somalia, the gauge coverage is dense (Fig. 3) and indicated rainfall on the order of 250 mm to over 400 mm, compared to 25 to 100 mm in the LTM (Fig. 1). Monthly anomalies were typically 50 to 200 mm.

In addition to northwest and central Kenya, drier conditions also prevailed in northern Somalia and Ethiopia, Eritrea, southern Sudan, parts of South Sudan, and central and southern Tanzania. In most of those areas October rainfall was on the order of 25 to 100 mm, but still above average.

Table 1 shows some of the more extraordinary rainfall totals at stations in eastern Africa. Mombasa, Kenya, one of the wetter stations with an October mean of 100 mm, received 528 mm. Kitui, Kenya, with an October mean of 83, received 554 mm. In Somalia, stations with October averages between 49 and 83 mm received 200 to 300 mm. Even coastal Mogadishu, with a mean of 30 mm, received 113 mm. Surprisingly, for most of the 36 Kenyan stations with available data (not shown), October 2019 did not come close to setting records. Rainfall exceeded the previous record at only three of the stations (Nairobi-Dagoretti, Kitui and Voi) and the difference was only a few tens of mm.

3.2. Central equatorial and western Africa

Fig. 3 also shows October rainfall over western areas. Positive anomalies of at least 20 mm were evident from at least 15° N to 14° S. Over West Africa the northern limit of the rainbelt was at roughly 15–17° N. The largest positive anomalies were over the Guinea Coast and in western equatorial Africa. Rainfall for the month was around 150–500 mm, some 50 mm to over 200 mm above the LTM. In southern areas of Benin and Togo, near the Atlantic coast, rainfall was 150% to over 200% of the LTM. In the northern areas, which are generally dry in October (Fig. 1), rainfall was on the order of 25–150 mm. This was some 20–50 mm above the LTM. Extensive rainfall deficits occurred only over the Guinea highlands in the far west, to the east of the Angolan highlands just south of the equator, and in parts of the Congo Basin. However, in most of central equatorial Africa and the Congo Basin anomalies were positive.

An interesting region of extreme positive anomalies was along the Atlantic coast of Gabon, the Republic of the Congo, the Democratic Republic of the Congo, and Angola. From roughly the equator to 15° S rainfall was on the order of 150% to over 300% of normal in a coastal strip spanning 3 to 4 degrees of longitude. Monthly totals exceeded 500 mm just south of the equator and were on the order of 200 to 400 mm elsewhere. This region is extremely sensitive to local SSTs, with large positive anomalies coinciding with unusual warming of coastal waters (Nicholson and Entekhabi, 1987). Notably, a strong positive SST anomaly occurred in October 2019 in the eastern Atlantic (see Section 5.5).

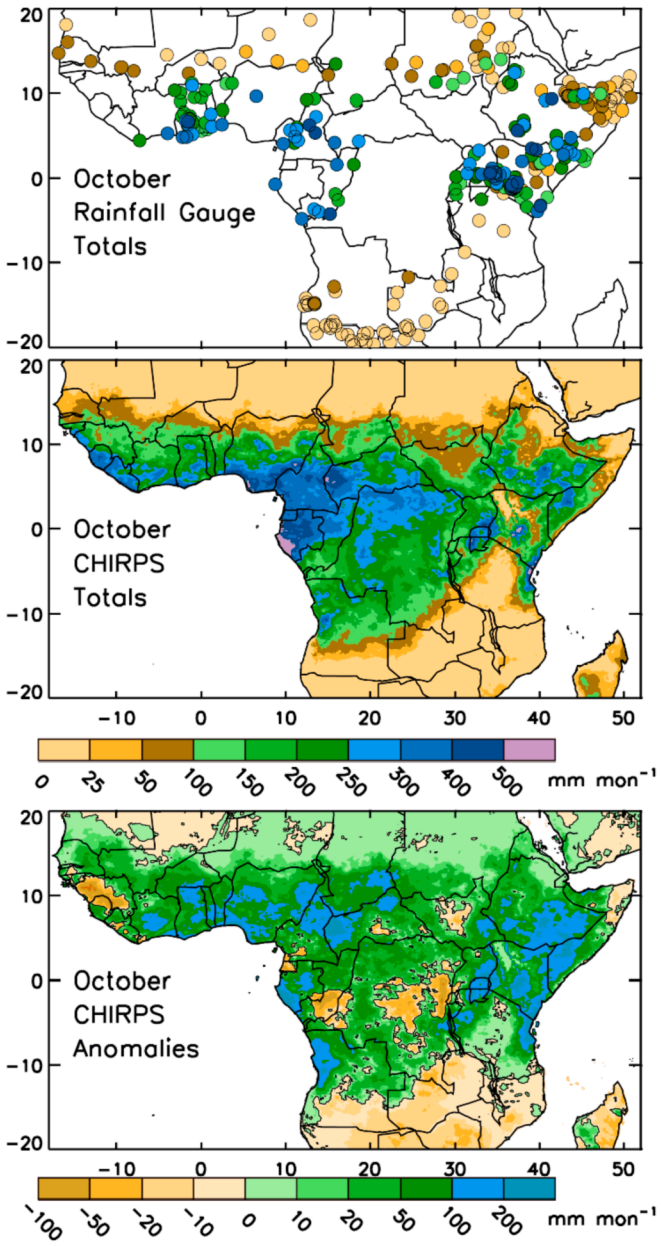

Fig. 3. October rainfall analysis. The top, middle and bottom rows show gauge observations, CHIRPS2 October totals, and the difference between CHIRPS2 and CHIRPS2 LTM.

4. Rainfall in November 2019

4.1. Eastern Africa

Climatologically, the rain belt is further south in November than in October (Fig. 1), so that on average November tended to be wetter than October in southern areas of eastern Africa but drier in northern areas (Fig. 4). In most of eastern Africa November rainfall was on the order of 50–100 mm, but considerably less to the far north. Western areas were wetter, as were central Kenya and areas near the coast.

November 2019 was exceptionally wet throughout a larger area than that occurring in October. Positive anomalies prevail from South Sudan and Ethiopia, around 8 to 15° N, to at least 20° S (Fig. 4). Again there is generally good agreement between gauges and CHIRPS2 except in northern Somalia, where the gauges show higher rainfall than CHIRPS2 (Fig. 4). The CHIRPS2 product uses a multiplicative scaling process, built around a long term mean, and this can limit its ability to capture extreme rainfall in places with low LTMs. In southern areas of Kenya, Uganda and Somalia and in northwestern Tanzania, rainfall was on the order of 250–500 mm, with departures from the LTM being on the order of 50 to over 200 mm. In two areas of central and northeastern Kenya (circa 2° N to 4° S), where November rainfall is typically 50 to 200 mm, November rainfall exceeded 400 to 500 mm.

Table 1
Rainfall at select stations in Kenya and Somalia during October 2019 compared to the long-term October mean (LTM) and the highest previous recorded value over the period of record for the station and year of occurrence.

Station	LTM	Oct 2019	Record (year)
Kenya			
Mombasa	100	528	825 (1997)
Embu	146	443	620 (1961)
Kitui	83	554	532 (1982)
Kisumu	68	341	233 (1995)
Malindi	67	363	391 (2009)
Dagoretti (Nairobi)	57	249	195 (1972)
Voi	28	159	150 (1951)
Lodwar	19	80	95 (2011)
Somalia			
Elberde	83	304	–
Sheikh	66	290	–
Bualle	63	244	–
Lugh Ferrandi	49	235	260 (1925)
Mogadishu	30	113	192 (1913)
Erigavo	10	62	21 (1948)

4.2. Central equatorial and Western Africa

Over central Africa and the two western sectors, the area of anomalously high rainfall was much smaller than in October. At least part of the change was due to the usual southward shift of the rain belt in November. The northern limit of the rain belt lies at roughly 5° to 7° N in November 2019. In the drier region to the north rainfall deficits were very weak. Rainfall was above average from roughly 5° or 10° N to 10° S in western sectors. Anomalies were on the order of 20–100 mm in most areas. The wettest conditions occurred in western equatorial Africa, between about 3° N and 5° S, and in southeastern Nigeria.

Rainfall deficits were evident along the Atlantic coast near the equator, to the east of the Angolan highlands, in a large swath west of the East African highlands (including the eastern Congo Basin), and south of about 10° S. Some of these areas experienced deficits in October as well. Deficits in the southern areas were as large as 100 mm or more.

5. Attribution of factors in the extraordinary rainfall of October and November 2019

5.1. Sea-surface temperatures

Fig. 5 shows maps of tropical SST anomalies for October and November of 2019. During both months, SST anomalies were predominantly positive throughout the equatorial and subtropical regions of the Atlantic and Indian Oceans. Pacific anomalies were positive north of the equator but negative south of the equator and weak in all regions. That, and the weak or positive correlations with SSTs in Niño 3.4 (Table 2) indicate that ENSO was not a factor in the rainfall anomalies of October/November 2019.

A feature to note is the area of strong positive SST anomalies along the eastern Atlantic coast of Africa during November, extending from Congo and Gabon southward through Angola. Anomalies were on the order of 1.5 to 3 °C. Overall, the SST anomaly pattern in both months strongly resembles the Atlantic Niño described by Lutz et al. (2013). Vallès-Casanova et al. (2020) have shown that 2019 was a particularly persistent Atlantic Niño, that extended into October/November and was

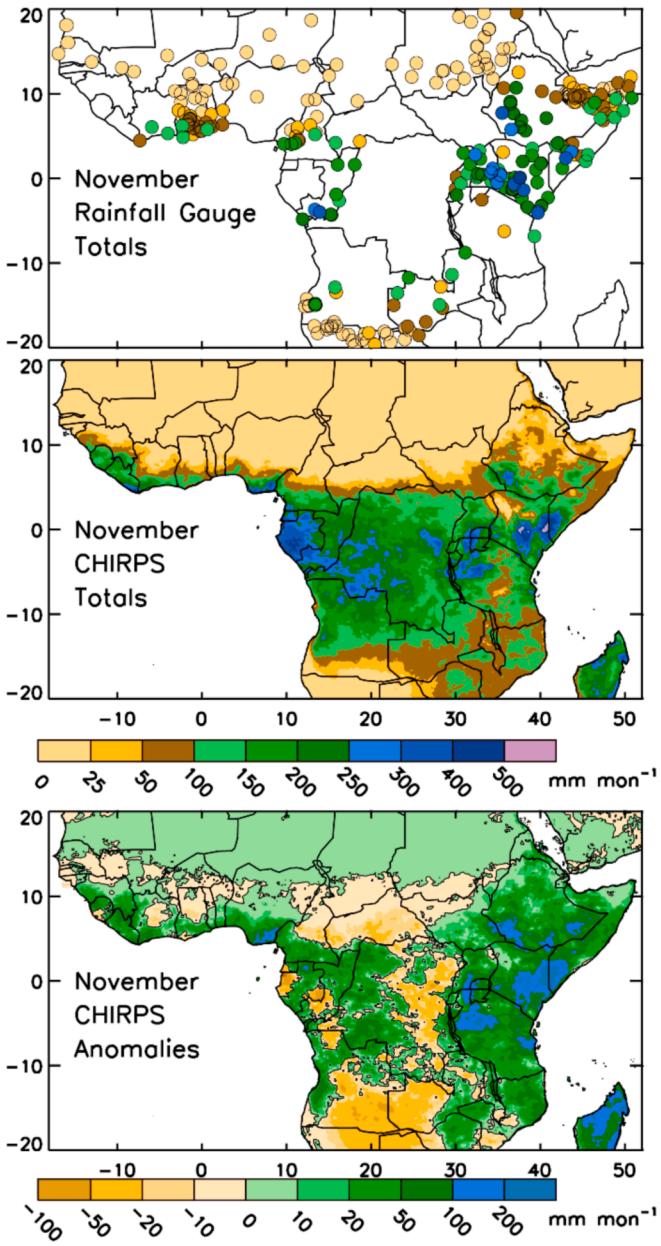

Fig. 4. As in Fig. 3, but for November 2019.

also particularly strong.

The time series of SSTs for the eastern Atlantic coastal region over the period 1950–2019 (Fig. 6a) clearly indicates the exceptional warmth in November 2019. The time series shown begins in 1950, due to concerns regarding data quality before that date. During this period the 2019 anomalies were the warmest on record. This is the Atlantic sector best correlated with rainfall in western equatorial Africa during October–November and it is also strongly correlated with rainfall in the Guinea Coast in those months (Nicholson et al., 2018a; Dezfuli and Nicholson, 2013). These SST anomalies most likely contributed to the positive rainfall anomalies in western equatorial Africa, particularly in areas near the coast, and in the Guinea Coast. Notably, SSTs in the equatorial Atlantic (6b) also reached a record high in both October and November, but nevertheless the temperature is just above the long-term mean, defined here as 1981 to 2010.

Over the Indian Ocean a strong dipole pattern is apparent in both October and November, with negative anomalies in the east and positive anomalies in the west. Notably, the western pole of the dipole is strongest well to the south of areas used to calculate the DMI, especially in November. The SST patterns indicate a weakening of the east-west SST gradient in both the equatorial Atlantic and the equatorial Indian Ocean. This is consistent with the weakening of the descending branch of the Walker cells in the equatorial Atlantic, as discussed later in Section 5.4.

The intense rainfall in western equatorial Africa and along the Guinea Coast can likely be attributed at least in part to the Atlantic SST anomalies. October–November rainfall in western equatorial Africa is strongly and positively correlated with SSTs along the coast of the eastern Atlantic (Nicholson and Entekhabi, 1987; Dezfuli and Nicholson, 2013; Lutz et al., 2015). The correlation with SSTs in the region east of 8° E and from the equator to 15° S is 0.65 for the period 1981–2010 (Table 2). The correlation with SSTs in the equatorial Atlantic (16° E-20° W, 5° N-5°S) over that period is lower (0.47) but still significant. The very strong link between Guinea Coast rainfall in the July-to-September season and SSTs in the Gulf of Guinea and the eastern equatorial Atlantic have been well established (e.g., Wagner and DaSilva, 1994; Opoku-Ankomah and Cordery, 1994; Okumura and Xie, 2004; Gu and Adler, 2004; Diatta and Fink, 2014; Nicholson et al., 2018a). Correlations for that season are as high as 0.75. The link to October–November rainfall is weaker but still significant: 0.48 for the coastal region of the eastern Atlantic mentioned above and 0.37 for the equatorial Atlantic.

The Atlantic SST anomalies of October and November 2019 probably did not play a strong role in the Sahel, central equatorial Africa, or East Africa. October–November rainfall in the Sahel shows little relationship with SSTs in the equatorial and eastern Atlantic (Nicholson et al., 2018a). The correlation during the period 1981 to 2010 is 0.10 with the equatorial Atlantic and 0.26 with the eastern Atlantic (Table 2).

The question of SSTs influencing rainfall in central equatorial Africa is complex because strong positive rainfall anomalies and strong negative rainfall anomalies are apparent in this region. Positive anomalies in the tropical Atlantic and tropical Indian Oceans have some tendency to inhibit rainfall in the Congo basin (Dezfuli and Nicholson, 2013; Balas et al., 2007). For the central equatorial African region shown in Fig. 2, the correlations of October–November rainfall are −0.34 and − 0.15 with the equatorial and eastern Atlantic SSTs, respectively (Table 2). They are similar for the Congo Basin sub-region. Thus, the positive Atlantic SST anomalies of October–November are consistent with the deficits noted in some sectors of central equatorial Africa. However, the prevailing rainfall anomalies are positive in those regions.

October–November rainfall in East Africa is not significantly correlated with rainfall over the Atlantic (Table 2), but it is strongly controlled by SSTs in the western Indian Ocean. Anomalously high Indian Ocean SSTs, as seen in Fig. 5, would be consistent with high rainfall (Ummenhofer et al., 2009).

5.2. The Indian Ocean dipole

Early studies suggested that ENSO was the main driver during the "short rains" season (e.g., Ropelewski and Halpert, 1987; Nicholson and Kim, 1997; Schreck and Semazzi, 2004), but more recent work has shown that the Indian Ocean Zonal Mode, or Indian Ocean Dipole (IOD), may be more important (Webster et al., 1999; Black et al., 2003; Slingo et al., 2005; Behera et al., 2005; Bahaga et al., 2019). The IOD is the SST difference between the eastern and western equatorial Indian Ocean, calculated for the sectors shown in Fig. 2. ENSO and the IOD tend to occur at the same time (Nicholson, 2015), so that a link of both factors to rainfall is evident. However, Fig. 5 indicates that in 2019, an extreme positive IOD event occurred during ENSO-neutral conditions.

Fig. 6c shows the DMI since 1950, based on the ERSST.v5 data set. Extreme positive values occurred in 1961, 1972, 1982, 1994, 1997, and 2006, all of which were very wet years in eastern Africa. The 2019 positive dipole event is the strongest since 1950 for both October and November. A comparison with data since 1874 published in Nicholson (2015) suggests it is one of the strongest on record, consistent with Ratna

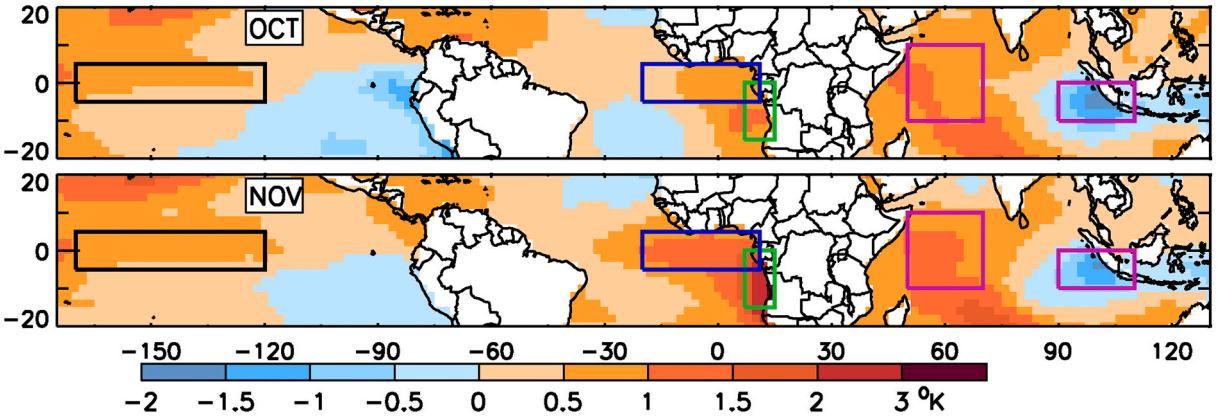

Fig. 5. SST anomalies during October and November 2019. Green and blue boxes indicate the areas for eastern Atlantic and equatorial Atlantic SST calculations; purple boxes indicate the areas for DMI calculation; see Fig. 6. Black box over Pacific Ocean is Nino 3.4. (For interpretation of the references to colour in this figure legend, the reader is referred to the web version of this article.)

Table 2
Correlation of regional October–November rainfall with Atlantic SSTs, the Dipole Mode Index (DMI) and Niño 3.4 SSTs. Ocean areas for which correlations are carried out are shown in Fig. 5. Except for the Congo Basin, the correlations are based on the period 1981 to 2010. Because of a dearth of recent gauge stations, that for the Congo Basin is based on the period 1964 to 1994. Regions are shown in Fig. 2.

Region (cf. Fig. 2)	Eastern Atlantic (cf. Fig. 5)	Equatorial Atlantic (cf. Fig. 5)	DMI	Niño 3.4
Guinea coast	**0.37**	**0.48**	0.20	0.12
Western equatorial Africa	**0.47**	**0.65**	0.20	−0.20
Central equatorial Africa	−0.15	**−0.34**	**0.58**	**0.39**
Congo Basin	−0.26	**−0.36**	**0.47**	0.26
East Africa	−0.23	0.03	**0.78**	**0.58**
Sahel	0.10	0.26	0.16	**0.31**

Correlations significant at the 0.05 level or better are shown in bold.

et al. (2020). Clearly, the dipole was a factor in the torrential rains in eastern Africa during both October and November (Wainwright et al., 2020). Notably, the DMI magnitude only slightly exceeded that of the 1994 in October and 1997 in November, months which in eastern Africa were considerably drier than in 2019. This suggests other factors might have come into play. It may have had an influence in central equatorial Africa, as positive correlations between the DMI and rainfall are apparent for that area and for the Congo Basin sub-sector (Table 2). The influence is strongest in the far eastern area (Dezfuli and Nicholson, 2013). However, as noted, there are both positive and negative rainfall anomalies within central equatorial Africa.

While the heavy rainfall in eastern Africa is likely to be attributed to the IOD, that is not the case with other areas affected. Pan-tropic SST/rainfall correlations presented by Nicholson et al. (2018b) suggest that October–November rainfall along the Guinea Coast is not associated with the IOD, while it might have a slight impact on October–November rainfall in the Sahel. This is confirmed by the correlations in Table 2. The relationship is also insignificant for the October–November gauge series for western equatorial Africa.

5.3. Zonal winds over the Indian Ocean

Hastenrath (2001, 2007) identified a physical mechanism by which the short rains are modulated on interannual time scales: a change in the low-level zonal winds over the central equatorial Indian Ocean. Anomalous surface westerlies over the central equatorial Indian Ocean, which are generally accompanied by anomalously weak upper-tropospheric easterlies, weaken the Indian Ocean Walker cell. This reduces the intensity of both the descending branch of the cell, which climatologically lies directly above eastern Africa and promotes aridity, and of the ascending branch in the eastern Indian Ocean. While a similar change occurs during most positive IOD events and many El Niño events, the zonal winds can contribute independent to the variability of the short rains. Moreover, the intensity of the low-level westerlies appears to be the most important factor involved in the variability of the short rains. The link is so robust that the correlation with October–November rainfall is −0.74 over the 139-year period 1874 to 2012 (Nicholson, 2015). Over the same period the correlation is 0.61 with the DMI and 0.49 with Niño 3.4.

Fig. 7a shows the vector wind anomalies at 925 hPa. The anomaly pattern over the central equatorial Indian Ocean is extremely clear and appears to be another common denominator in October and November 2019. Strong easterly anomalies appear in a large sector from 60° E to 100° E and 5° N to 5° S in both months. In fact, the westerlies were replaced by easterlies (not shown) with speeds on the order of 10 ms^{-1} in most of that sector. This appears to be related to the fact that the absolute value of the east-west Indian Ocean gradient was close to zero, due to the extremely warm western Indian Ocean sea surface temperatures combined with the abnormally cool eastern Indian Ocean anomalies. At 150 hPa (Fig. 7b) a weakening of the easterlies is also apparent in both months. However, the anomaly is weaker than at 925 hPa. In the indicated box the speed of the mean zonal wind at 150 hPa in both months is only two to four ms^{-1} below the LTM for 1979 to 2019. The changes at both levels are consistent with the mechanism described by Hastenrath (2007).

5.4. The walker circulation

The Walker Circulation is examined by way of both vertical velocity (omega) and streamlines. Two dimensional (longitude-by-height) maps of vertical velocity and streamlines can be used to assess the location and strength of the African Walker circulation cells. Areas with low-level converging streamlines and mid-level upward velocities will typically experience heavy precipitation. Fig. 8 shows the October LTM, October 2019 values, and the difference between 2019 and the LTM. Fig. 9 shows the same for November 2019. Omega indicates that in the LTM for both October and November the descending branch of the Indian Ocean Walker cell is very pronounced (top frames). Over eastern Africa (near 30° E to 45° E) subsidence prevails in the mid- and upper troposphere. This subsidence serves to suppress rainfall. In contrast, during 2019 (middle frames) the descending branch is extremely weak overall, especially in November, and absent in the lower to mid-troposphere. The

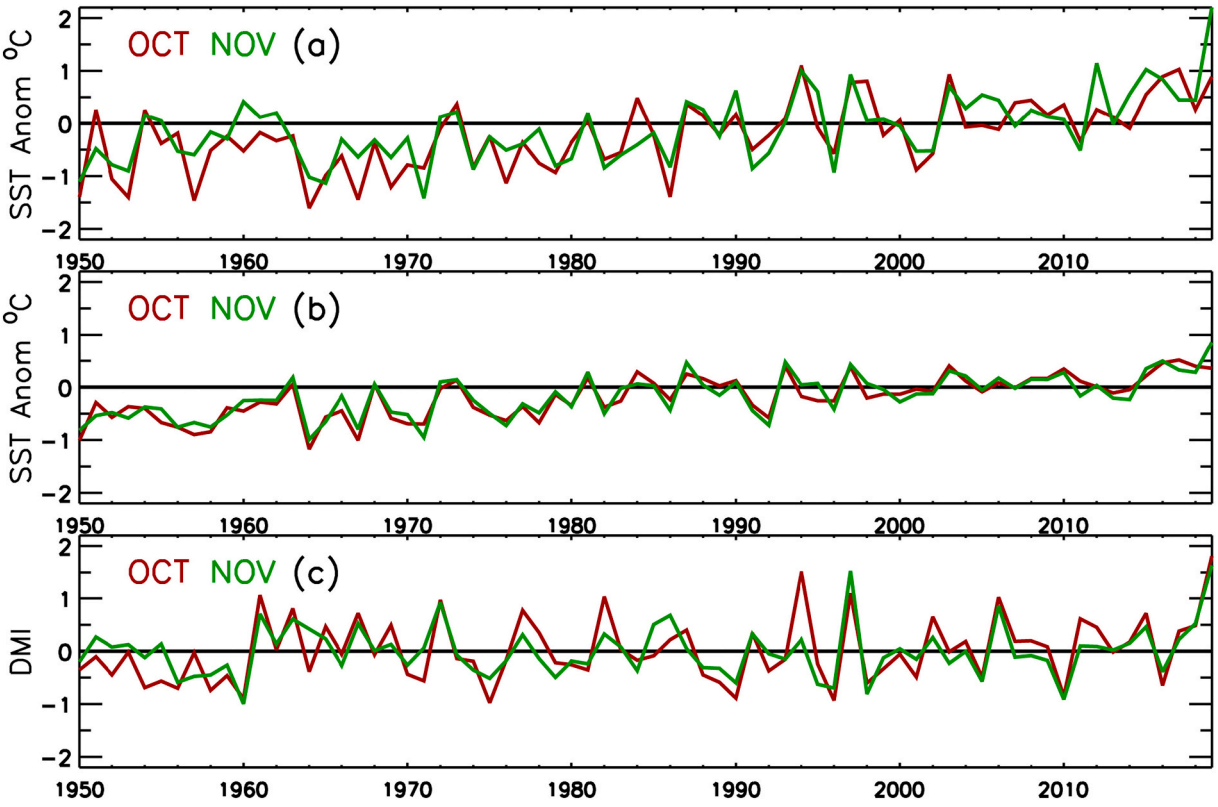

Fig. 6. a. Time series of SST departures from the 1981–2010 mean, averaged for the green box indicted in Fig. 5 in the eastern Atlantic. (For interpretation of the references to colour in this figure legend, the reader is referred to the web version of this article.)
b. As in 6a, but averaged for the blue box indicted in Fig. 5 for the equatorial Atlantic.
c. The DMI time series for October and November, calculated as the difference between the western and eastern boxes shown in purple in Fig. 5.

blue columns in the bottom frames from roughly 30° E to 60° E illustrate this reduction. The reduction of subsidence is particularly noteworthy, as this has been shown to be a major factor in the interannual variability of the short rains (Hastenrath et al., 2011).

The Walker-type circulation anomalies as evident in the omega fields are also consistent with the rainfall anomalies elsewhere in equatorial Africa. During October the region of ascent over equatorial Africa (roughly 30° E to 0°) was abnormally broad and intense. The difference field shows that the area of reduced subsidence or increased ascent extends to the west coast of the continent. However, these changes were not completely uniform. The difference fields also indicate reduced ascent in the lower to mid-troposphere from roughly 30° E to 15°E. That span coincides with areas of rainfall deficits shown in Fig. 3. In November, the situation is different. Although subsidence was greatly decreased over eastern Africa, contrasts between the LTM and November 2019 were very weak in most other areas. This is consistent with the relatively weak or negative rainfall anomalies in central and western equatorial regions.

Streamline anomalies for October and November (Figs. 8c and 9c) confirm the changes suggested by the omega fields. During October, streamline anomalies suggest increased vertical motion in most areas from roughly 15° W to 70° E, but anomalies were particularly strong from around 15° E and 10° W. A small area of decreased ascent at low-levels resides at around 25–30° E and corresponds to the area of rainfall deficits over the Congo Basin (Fig. 1). The streamline anomalies over Africa are similar in November, except that the negative anomalies between 30° E and 10° E are strong and more vertically extensive than during October. This is consistent with the larger area of rainfall deficits over the Congo Basin in November. Note that in November, subsidence anomalies over the eastern Indian Ocean and the Maritime Continent have strengthened compared to the October anomalies (Figs. 8c and 9c).

To more closely examine the patterns of vertical motion related to the anomalies over the Guinea Coast and western Sahel during October, omega profiles were calculated for 0° to 10° N, eliminating the extensive ocean area to the south. For the sake of brevity this analysis is not shown. However, it not only confirmed the results shown in Fig. 8 but showed much stronger ascent in the longitudes between 5° E to 15° W than was evident in the profile for 10° N to 10° S. That stretch includes most of the Guinea Coast.

5.5. *Moisture flux and divergence*

Fig. 10 shows anomalies in total atmospheric moisture flux (vectors) and moisture flux divergence (colors) during 2019. Moisture flux vectors describe the path taken by atmospheric water vapor. Areas with moisture flux divergence will typically not be rainy. Areas with extensive moisture flux convergence are typically rainy. The local moisture budget ensures that moisture convergence equals precipitation minus evaporation, so there is a tight coupling between convergence and precipitation. In October the moisture flux anomaly was almost ubiquitously easterly within eastern Africa and moisture convergence was anomalously strong throughout the region. The areas of strongest moisture convergence corresponded closely to the areas with the highest rainfall anomalies (Fig. 3). This suggests that convection may have been enhanced by abundant moisture and moist instability.

Likewise, anomalous convergence coincided with the areas of anomalously high rainfall over the Guinea Coast, much of the western Sahel, and western equatorial Africa (Gabon and western areas of Congo and Angola). The very warm SSTs noted in 5.1 helped set the stage for this situation. The increase in moisture flux and flux convergence was particularly strong over the Guinea Coast. The increase in moisture flux was from a westerly to southwesterly direction, which means advection

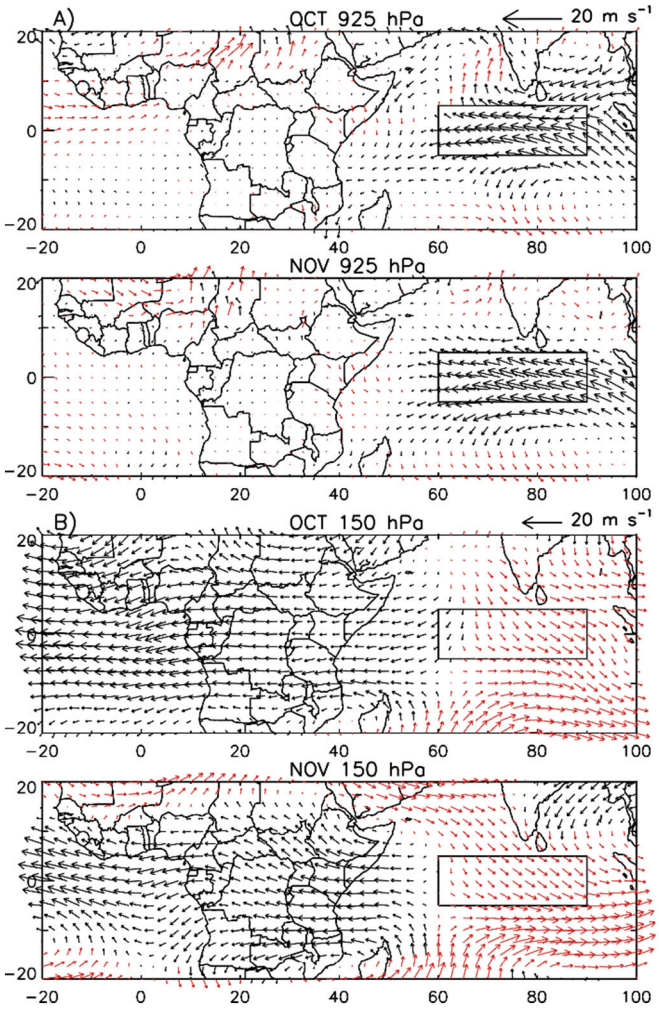

Fig. 7. a. Vector wind anomalies at 925 hPa: October and November 2019 minus the 1981–2010 mean for these months. Westerly anomalies are in red. The rectangle in the central Indian Ocean shows the area where zonal wind anomalies are closely linked to October–November rainfall in eastern Africa. 7b. As in Fig. 7a, but for 150 hPa. (For interpretation of the references to colour in this figure legend, the reader is referred to the web version of this article.)

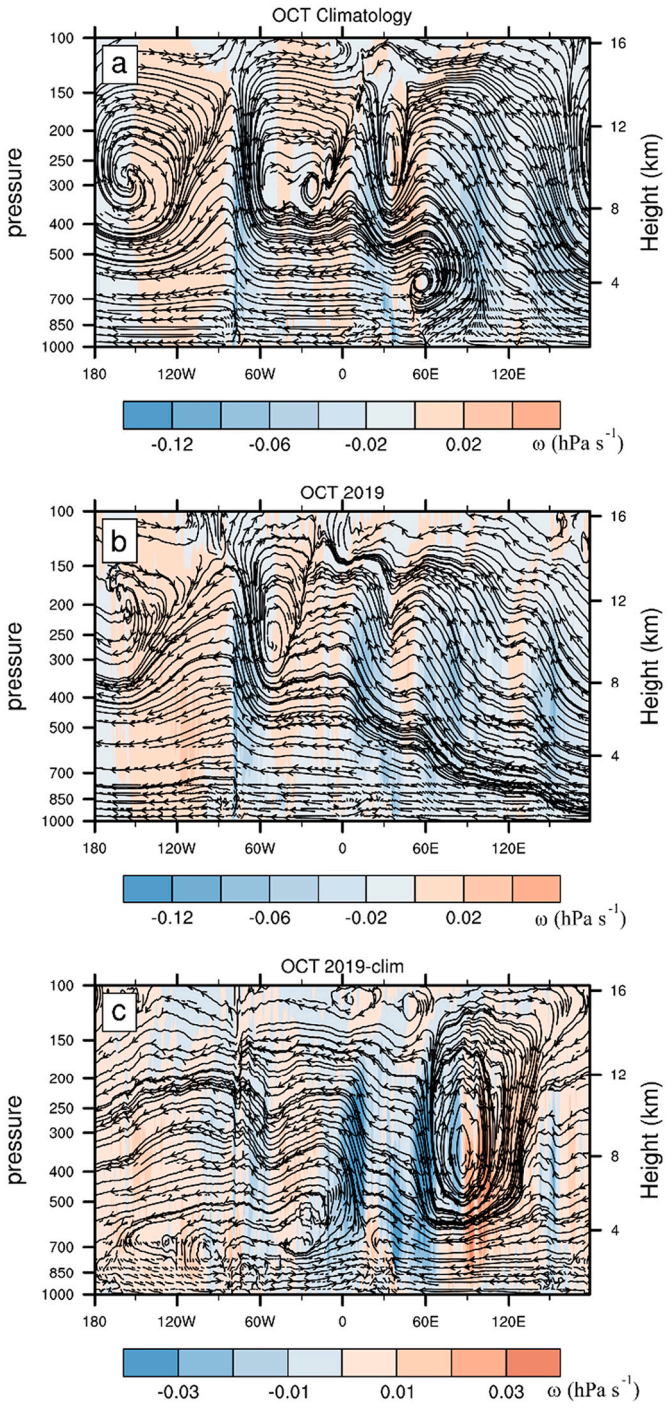

Fig. 8. Streamlines (arrows) and omega (vertical motion, colors) for October 2019, averaged between 10° N and 10° S. Top panel: climatology. Middle panel: October values. Bottom panel: October anomalies (October-minus-climatology). Blue indicates upward motion or increased ascent and tan indicates downward motion or decreased ascent. (For interpretation of the references to colour in this figure legend, the reader is referred to the web version of this article.)

of moist air from the Atlantic into the region. In addition to the warm SSTs, there was also an anomalous meridional mean sea-level pressure (MSLP) gradient in the central African Sahel between lower MSLP over the eastern Sahara and higher pressure between 10 and 15°N. That enhanced of the transport moist air zonally into the central Sahel (Fig 11). In accordance with the largest northward displacement of the Intertropical Discontinuity (ITD) and the 35 mm isopleth of the total column water vapor was observed over this region (Fig. 11). It is interesting to note that (a) a similar pressure and westerly moisture flux anomaly was observed over Chad and Sudan in August 2020 when extreme rainfall and flooding occurred in the later country (Elagib et al., 2021) and (b) that recent wetting in the Sahel is concentrated in the late rainy season and away from the West Coast (Nicholson et al., 2018a; Biasutti, 2019).

Over western equatorial Africa flux anomalies were considerably weaker and from an easterly direction, bringing in moisture from the Congo rain forest region. However, flux convergence was anomalously strong. A few areas of reduced moisture flux convergence/increased divergence over Cameroon in the east and the Guinea highlands in the west roughly coincide with areas of rainfall deficits during October 2019.

The situation was very different over central equatorial Africa. To the north, where rainfall anomalies were strongly positive, there was increased flux convergence and strong positive flux anomalies from the west. Elsewhere in October moisture flux and flux convergence were weak and spatially heterogeneous. However, there is a tendency for increased flux and flux convergence in areas of positive rainfall anomalies and decreased flux and flux divergence in areas of rainfall deficits, such as the central Congo Basin.

In November, the anomalies in moisture flux were extremely weak

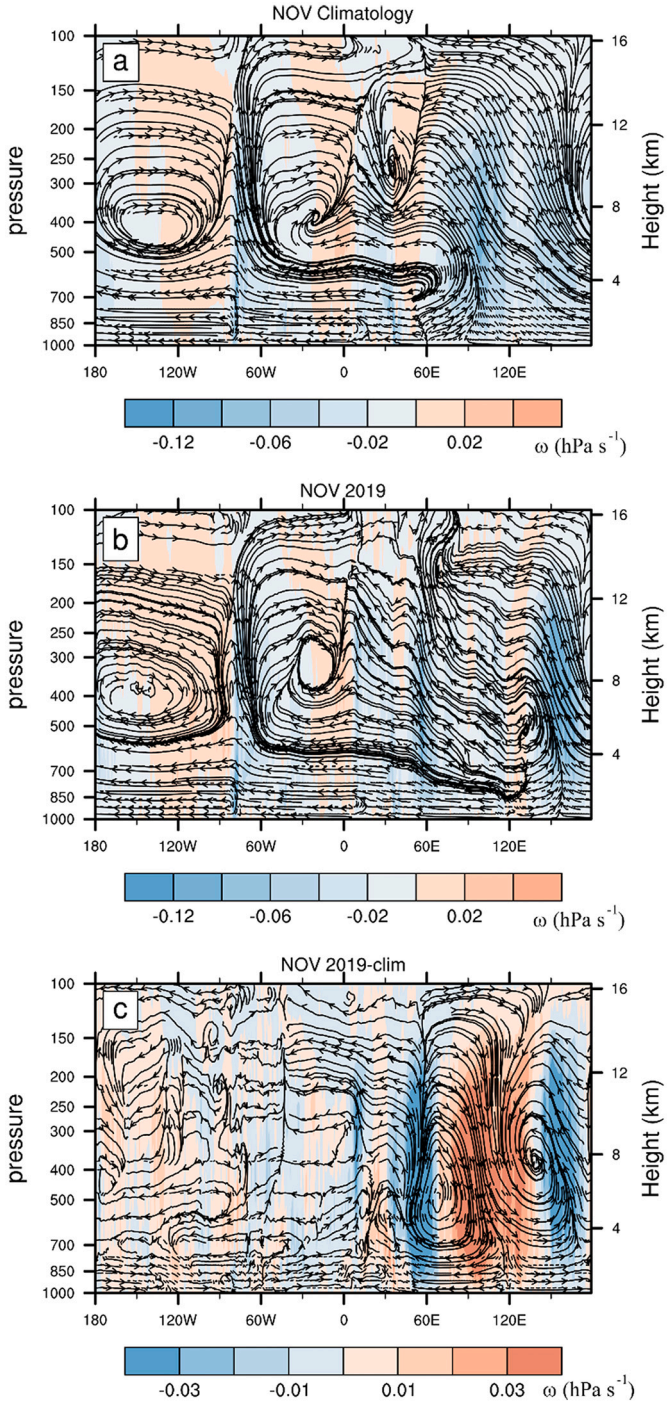

Fig. 9. As in Fig. 8, but for November 2019.

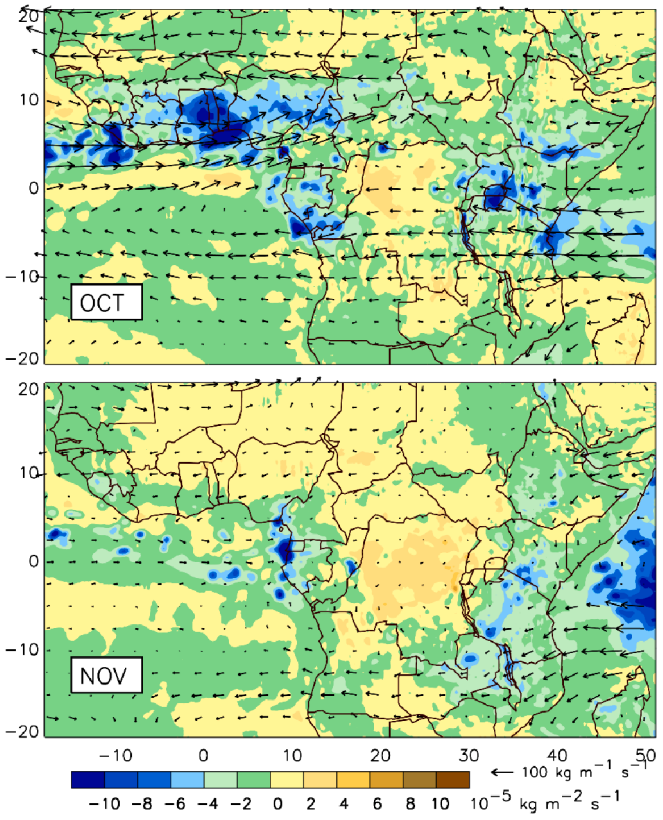

Fig. 10. Anomalies of vertically-integrated atmospheric moisture flux (vectors) and moisture flux divergence (colors) during October and November 2019.

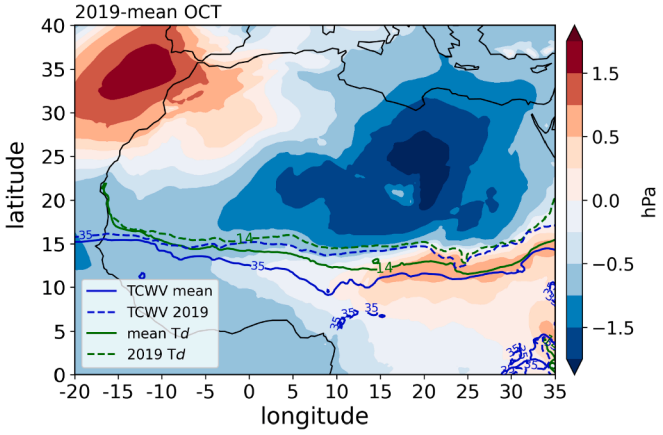

Fig. 11. Anomalous state of the West African monsoon in October 2019. Mean sea-level pressure anomalies with respect to the 1981–2010 mean (colored), mean (solid green) and Oct. 2019 (dashed green) location of the Intertropical Discontinuity evidenced by the 14 °C 2-m dew point temperature contours, and mean (solid blue) and Oct. 2019 (dashed blue) location of the 35 mm total column water vapor isopleths.

over eastern Africa, potentially indicating that rainfall was easily triggered locally in a pre-existing moist troposphere, as evident from anomalies of total precipitable water (not shown). Exceptions were in southern Tanzania and northern Mozambique, and the far north of Somalia. Positive anomalies in moisture flux convergence are evident over most of the region. However, negative anomalies prevail in areas of southeastern Ethiopia, western Somalia, and northeastern Kenya that have the strongest rainfall anomalies. Notably, the anomalies in both flux and flux convergence were considerably weaker than during October 2019. Positive anomalies in moisture flux convergence are evident over the regions of the Atlantic coast and eastern Africa that experienced anomalously high rainfall. However, over central equatorial Africa and parts of western equatorial Africa, negative flux anomalies cover a vast area, including many locations with strong positive rainfall anomalies.

5.6. *Jets and tropical waves*

Fig. 12 shows the zonal profile of wind during October 2019 and also the LTM at 0° W and 15° E. At 0° W the AEJ-N was displaced some 2.5° north of its LTM position and the TEJ, which is not evident in the mean,

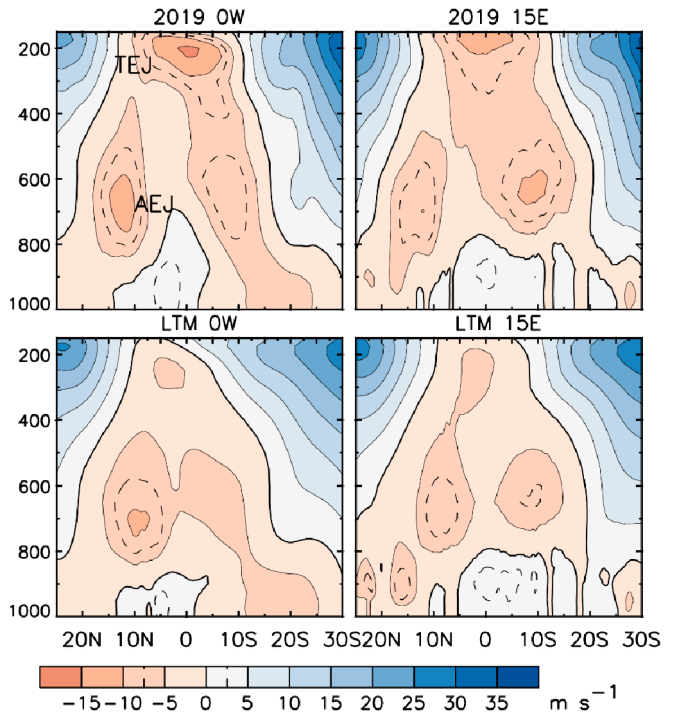

Fig. 12. Vertical profile of zonal wind at 0° W (left) and 15° E (right) during October 2019 and the LTM. Positive values correspond to westerlies.

was well-developed. The low-level westerlies were also abnormally strong and extended up to 700 hPa. Similar changes are evident also at 15° E, although the more extensive westerlies are only evident in the northern-hemisphere latitudes. These changes are all associated with increased rainfall in western equatorial Africa during the boreal autumn. In November zonal wind anomalies were relatively small and hence not shown. There was a slight northward displacement of the AEJ-N, but neither low-level westerlies nor the TEJ developed.

Papers by Nicholson and Webster (2007) and Cook (2015) discuss an inertial instability mechanism that might be responsible for the northward shift of the AEJ-N. Both papers linked this displacement and increased Sahel rainfall to an enhanced low-level meridional pressure gradient and enhanced intensity of the Saharan heat low, however they considered mainly the boreal summer season. It remains open if such an instability mechanism can operate so late in the season. The instability parameter used in Cook (2015) increased towards October–November 2006 and was well above the critical value of zero. However, in line with the intensified AEJ-N, the intensity of the meridional pressure gradient and the Saharan heat low were anomalously strong in October 2019 (cf. Fig. 11).

The northward displaced and enhanced AEJ-N in October can also be seen in Fig. 13, which shows October 2019, LTM, and anomalous 700-hPa zonal wind speed. The AEJ-N axis is also associated with anomalous 2–6-day bandpass-filtered 700 hPa meridional wind variance, traditionally used as an indicator for African Easterly Wave activity (Reed et al., 1977). And AEWs are known to be related to squall line activity in West Africa (Fink and Reiner, 2003), thus suggesting that an unseasonally strong northward position of the AEJ-N, providing anomalous low-level wind shear and enhanced AEW activity, triggered more organized rainfall systems in the Sahel and Guinea Coast (cf. Maranan et al., 2018; Klein et al., 2021). Another enhanced zone of 2–6-day bandpass filtered, 700-hPa meridional wind variance is located over the Gulf of Guinea in an area of minimum easterly wind speed, thus suggesting that the cross-equatorial meridional wind fluctuated with AEW activity in the north.

In western and central equatorial Africa Kelvin waves are known to

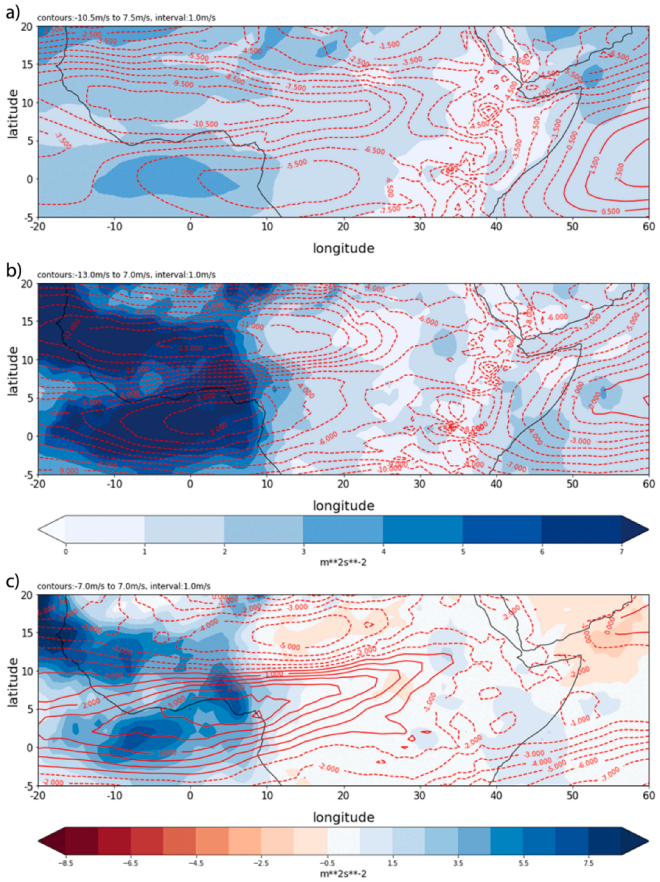

Fig. 13. 700-hPa zonal wind (contours, in m/s) and 2–6 bandpass-filtered meridional wind variance (colors, in mˆ2/sˆ2) for October 2019. Top panel: climatology. Middle panel: October 2019 values. Bottom panel: October anomalies (October 2019-minus-climatology). Blue indicates enhanced meridional wind variance in the periodicity typical for AEWs. (For interpretation of the references to colour in this figure legend, the reader is referred to the web version of this article.)

be related to rainfall fluctuations (Laing et al., 2011; Sandjon et al., 2014; Sinclaire et al., 2015; Jackson et al., 2019), while the MJO impacts rainfall over eastern equatorial Africa (e.g., Pohl and Camberlin, 2006). Based on the local wave amplitude approach presented in van der Linden et al. (2016) and Schlueter et al. (2019), we introduce a novel wave phase-amplitude diagram that allows for an assessment of local tropical wave amplitudes. Fig. 14 shows that at the end of November, a Kelvin wave passed from west to east over Africa that in its local wet phase (P5) belonged to one of the strongest, if not the strongest, based here on wave-filtered IMERG rainfall data since at least the year 2000. This can be seen in Fig. 14 by the fact that its local wave amplitude temporarily exceeded the 99th percentile in the wet phases P4, P5 and P6 of the Kelvin wave. Interestingly, the local wet phase of the MJO co-occurring at the same time also belonged to one of the strongest in the last 20 years (Fig. 14), suggesting a constructive wave interference in the last decade of November that was also very wet at stations in Kenya (not shown). However, local MJO standardized amplitude was below one during the wet phase in October, not supporting Wainwright et al. (2020)'s notion of a dominant role of MJO in that month.

6. Summary and conclusions

The flood situation of October–November 2019 was extraordinary in that it involved nearly all of equatorial Africa - a region that is not historically homogeneous. Unusually heavy rainfall affected eastern Africa during both months, but more western regions were impacted

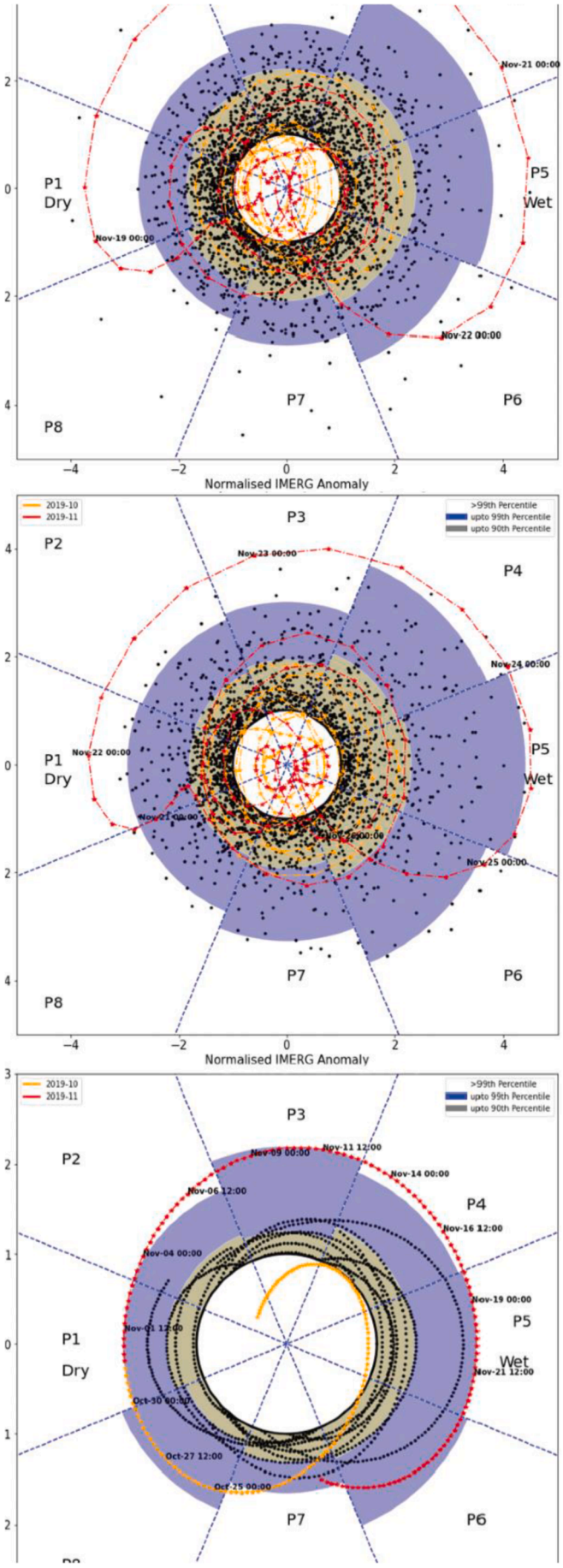

(caption on next page)

Fig. 14. Phase-amplitude diagram showing the local amplitudes of Kelvin waves (top two panels) at 10°E and 40°E and MJO (bottom panel) at 40°E for October–November 2019. The tropical waves are based on the Wheeler and Kiladis (1999) wave filtering of six-hourly IMERG rainfall data in the equatorial belt between 5°N-5°S. The eight phases are defined as in van der Linden et al. (2016), with Phase 1 (7) being the local dry (wet) phases. Colors represent the local normalized wave amplitudes larger than one with the two colors representing the 90th and 99th percentile of the phase-dependent wave amplitude. Red dots connected by lines are dates in October–November 2019, black dots are dates in all other October–November months since 2000. (For interpretation of the references to colour in this figure legend, the reader is referred to the web version of this article.)

during October, when strong positive rainfall anomalies prevailed from 15° N to 10° S. October anomalies were in eastern Africa and in the Sahel, where rainfall was some 200–400% of the LTM. Kenya and Tanzania were particularly hard hit. In wetter locations, rainfall was some 150–200% of the LTM. The few areas with rainfall deficits were east of the Angolan highlands, the Congo Basin, the northern tip of Somalia, the Guinea highlands, and few other small isolated areas.

In November, when the rainbelt lies considerably further south, the area of positive anomalies lay further south and fewer areas experienced anomalously high rainfall. Rainfall was still unusually high throughout eastern Africa, with rainfall on the order of 200% to over 400% of the LTM. The most extreme conditions were over Somalia and Ethiopia. In the Guinea Coast rainfall was above normal only in the most southern areas. Rainfall was above normal in most of western equatorial Africa and in western parts of central equatorial Africa, but only in the latitudinal span of c. 5° N to 12° S. Anomalies were generally less than 150% of normal.

The flood situation appears to be linked to a simultaneous occurrence of an Indian Ocean Dipole event and an Atlantic Niño. Consistent with Ratna et al. (2020), the dipole event is the strongest since at least 1950 and possibly the strongest on record. The magnitude of the SSTs along the eastern coast of the equatorial Atlantic suggests that may have also been a record-breaking Atlantic Niño.

The high rainfall in eastern Africa can clearly be attributed to the Indian Ocean Dipole, and associated changes in the zonal winds over the central equatorial Indian Ocean. The net result was a dramatic decrease in the subsidence over eastern Africa. This subsidence is associated with the descending branch of the Indian Ocean Walker cell. A very similar situation prevailed during both months. Despite that, November rainfall anomalies over most of eastern Africa were notably smaller than during October. Increased moisture flux and flux convergence likely played a role in October but was less of a factor in November. However, during late November record-breaking wet phases of MJO and Kelvin waves contributed to the wetness in this month. This wave activity might also help to explain the extreme November anomalies in the Horn of Africa. Climate scale conditions (the IOD) conspired with intra-seasonal weather patterns (MJO and Kelvin waves) to produce extreme zonal wind and rainfall outcomes. However, our analysis does not support a major role of the MJO in October 2019 as mentioned in Wainwright et al. (2020). Increased moisture flux and convergence may have contributed to the large positive rainfall anomalies over southern Tanzania and northern Mozambique.

Our diagnosis of the November extremes could inform improved early warning systems. For drought monitoring, there is an emerging consensus that 'staged' or 'telescoping' prediction systems can be used to effectively combine climate and weather information. In retrospect, one might imagine that observed and/or predicted DMI values could have been used to place East Africa on alert. Forewarned, these nations would have been better situated to make use of downscaled weather forecasts (e.g. https://chc.ucsb.edu/data/chirps-gefs), which appear to have anticipated fairly well the late November extreme rainfall totals (not shown).

It should be stressed however, that analyzing the Walker circulation using an equatorial cross section of streamlines and vertical motions is not quantitative and needs further study regarding cause and effect. A promising approach is that presented in Schwendike et al. (2014) that separates the mass circulations associated with local Walker and Hadley cells. In eastern equatorial Africa, the anomalous rains extended beyond the October–November period into December 2019 and January 2020. Four tropical cyclones in the Indian Ocean in December 2019 may have been a contributing factor in the high rainfall of that month (Finney et al., 2019; Wainwright et al., 2020). Thus future studies focusing on the Greater Horn of Africa should include December 2019 and January 2020.

The meteorology of central equatorial Africa has been critically understudied (Creese and Washington, 2018) and it is this region that is least understood from a meteorological point of view. Moreover, most recent research on the region (e.g., Hua et al., 2016) has focused on the boreal spring season because of the long dry trend. It is also the region with the weakest links to large-scale phenomena (Dezfuli and Nicholson, 2013). Evidence of this phenomenon is the extremely high spatial variability of rainfall over the Congo Basin, compared to other regions in tropical Africa (Nicholson, 2021). This lack of spatial coherence is consistent with the occurrence of rainfall deficits when elsewhere extremely positive anomalies prevail.

Not surprisingly, a clear set of factors contributing to the October–November anomalies in the Congo Basin did not emerge from our work. A significant positive correlation is apparent with the Indian Ocean Dipole. However, in this region, areas of excess and deficit rainfall were apparent. Increased/reduced moisture flux convergence tended to correspond to positive/negative rainfall anomalies. Increased subsidence probably contributed to areas with deficits. Positive SST anomalies over the equatorial Atlantic may have contributed to the negative rainfall anomalies, as well. Overall, however, large-scale forcings are weak in this area. An explanation for this, and for the low spatial coherence, might be found in the low convective inhibition prevalent over the Congo basin over large parts of the year. This allows for quite randomized convective outbreaks, which due to the low wind shear often do not organize into large-scale propagating systems.

The IOD was not a factor in the anomalously high rainfall outside of East Africa. In western and central equatorial regions, the operative factors are not very clear but several may have been involved. For western equatorial Africa the most important was very likely the exceptionally high SSTs along the coast of the eastern Atlantic. The positive SST anomalies elsewhere are more likely to inhibit rainfall. The intensification of the TEJ and the low-level westerlies to the west of the region probably also contributed to increased rainfall.

For the Guinea Coast and western Sahel, where the flood situation was pretty much limited to October, the most important factor was arguably the wind and AEW regimes: the development of strong equatorial westerlies and the Tropical Easterly Jet and northward displacement of the African easterly jet that also lead to enhanced and northward-displaced AEW activity. We speculate that the anomalously high SSTs in the equatorial Atlantic, as underscored in the time series in Fig. 9, played a role in producing these changes. High rainfall in the Guinea Coast was also favored by the strong positive SST anomalies along the eastern coast of the Atlantic. An additional factor was a strong increase in moisture flux from the Atlantic and increased moisture convergence. All this can be interpreted as a later than usual retreat of the West African monsoon, which is a possible climate future at the end of the century (Biasutti, 2013; Monerie et al., 2016).

In summary, the present study documents for the first time the pan-African wetness in the equatorial belt in October–November 2019, which can be attributed to the juxtaposition of several factors. The Indian Ocean Dipole was clearly a major factor in eastern Africa, along with moisture transport into the region and very strong November

Kelvin wave and MJO activity. Record-breaking tropical Atlantic SSTs were probably a major factor for the three western-most regions, particularly the strong coastal anomalies. The warming in the equatorial Atlantic, abetted by an anomalously strong thermal low over the Sahara, may have played a role in delaying the retreat of the West African monsoon, leading to positive rainfall anomalies over the Sahel and Guinea Coast. The current article paves the way to further analyses. They should include moisture and (moist static) energy budget approaches, quantitative assessments of the mass circulation of the Walker and Hadley cells, and modelling approaches.

Supplementary data to this article can be found online at https://doi.org/10.1016/j.gloplacha.2021.103687.

Declaration of Competing Interest

The authors declare that they have no known competing financial interests or personal relationships that could have appeared to influence the work reported in this paper.

Acknowledgements

First, we thank the two anonymous reviewers for the critical and helpful comments that helped to improve the manuscript. We also thank various colleagues, projects and services in Africa for providing station data, as well as the Deutsche Wetterdienst. Larisa Seregina provided one of the figures. We acknowledge also helpful discussion with Dr. Roderick van der Linden. SEN and DAK were supported by two grants from the National Science Foundation, GEO/ATM 1854511 and EAR 1850661. The second author acknowledges support from the Transregional Collaborative Research Center SFB/TRR 165 "Waves to Weather" (www.wavestoweather.de) funded by the German Research Foundation (DFG)." CF was funded by the U.S. Geological Survey Drivers of Drought and the Famine Early Warning Systems Network programs, U.S. Geological Survey (USGS) cooperative agreement #G14AC00042, United States Agency for International Development (USAID) cooperative agreement #72DFFP19CA00001, and National Aeronautics and Space Administration (NASA) Global Precipitation Measurement mission grant #80NSSC19K0686.

The analyses were based on data sets already in the public domain, as indicated in the text, and on gauge data, some of which is too new to have been placed in an archive. Anyone wishing to obtain the gauge data should contact one of the authors.

References

Anyah, R.O., Semazzi, F.H.M., 2006. Climate variability over the Greater Horn of Africa based on NCAR AGCM ensemble. Theor. Appl. Climatol. 86, 39–62.

Bahaga, T.K., Fink, A.H., Knippertz, P., 2019. Revisiting interannual to decadal teleconnections influencing seasonal rainfall in the Greater Horn of Africa during the 20th century. Int. J. Climatol. 39, 2765–2785.

Balas, N., Nicholson, S.E., Klotter, D., 2007. The relationship of rainfall variability in west Central Africa to sea-surface temperature fluctuations. Int. J. Climatol. 27, 1335–1349.

Behera, S.K., Luo, J.J., Mason, S., Delecluse, P., Gualdi, S., Navarra, A., Yamagata, T., 2005. Paramount impact of the Indian Ocean dipole on the East African short rains: a CGCM study. J. Clim. 18, 4514–4530.

Biasutti, M., 2013. Forced Sahel rainfall trends in the CMIP5 archive. J. Geophys. Res. 118, 1613–1623. https://doi.org/10.1002/jgrd.50206.

Biasutti, M., 2019. Rainfall trends in the African Sahel: Characteristics, processes, and causes. Wiley Interdiscip. Rev. Clim. Chang. 10 https://doi.org/10.1002/wcc.591.

Black, E., Slingo, J., Sperber, K.R., 2003. An observational study of the relationship between excessively strong short rains in coastal East Africa and Indian Ocean SST. Mon. Weather Rev. 131, 74–94.

Cai, W., Zheng, X.-T., Weller, E., Collins, M., Cowan, T., Lengaigne, M., Yu, W., Yamagata, T., 2013. Projected response of the Indian Ocean Dipole to greenhouse warming. Nat. Geosci. 6, 999–1007.

Cai, W., Santoso, A., Wang, G., Weller, E. Collins, Wu, L., Ashok, K., Masumoto, Y., Yamagata, T., 2014. Increased frequency of extreme Indian Ocean Dipole events due to greenhouse warming. *Nature* 510, 254–258.

Cattani, E., Merino, A., Guijarro, J.A., Levizzani, V., 2018. East Africa rainfall trends and variability 1983-2015 using three long-term satellite products. Remote Sens. 10 https://doi.org/10.3390/rs00060931.

Cook, K.H., 2015. Role of inertial instability in the West African monsoon jump. J. Geophys. Res. Atmos. 120, 3085–3102. https://doi.org/10.1002/2014JD022579.

Creese, A., Washington, R., 2018. A process-based assessment of CMIP5 rainfall in the Congo Basin: the September-November rainy season. J. Clim. 31, 7417–7439.

Dezfuli, A.K., Nicholson, S.E., 2013. The relationship of interannual variability in western equatorial Africa to the tropical oceans and atmospheric circulation. Part II. The boreal autumn. J. Clim. 26, 66–84.

Diatta, S., Fink, A.H., 2014. Statistical relationship between remote climate indices and West African monsoon variability. Int. J. Climatol. 34, 3348–3367.

Dinku, T., Funk, C., Peterson, P., Maidment, R., Tadesse, T., Gadain, H., Ceccato, P., 2018. Validation of CHIRPS satellite rainfall estimates over eastern Africa. Quart. J. Roy. Meteor. Soc. 144, 292–312.

Elagib, N.A., Al Zayed, I.S., Gayoum Saad, S.A., Mahmood, M.I., Basheer, M., Fink, A.H., 2021. Devilitating floods in the Sahel are becoming frequent. J. Hydrol. 599, 126362.

Emori, S., Brown, S.J., 2005. Dynamic and thermodynamic changes in mean and extreme precipitation under changed climate. Geophys. Res. Lett. 32, L17706.

Fink, A.H., Reiner, A., 2003. Spatio-temporal variability of the relation between African easterly waves and West African squall lines in 1998 and 1999. J. Geophys. Res.-Atmos. 108 (D11) https://doi.org/10.1029/2002JD002816. ACL 5-1–5-17, 4332.

Finney, D.L., Marsham, J.H., Walker, D.P., Birch, C.E., Woodhams, B.J., Jackson, L.S., Hardy, S., 2019. The effect of westerlies on East African rainfall and the associated role of tropical cyclones and the Madden–Julian oscillation. Quart. J. Roy. Meteor. Soc. 146, 647–664.

Funk, C., 2021. Drought Flood Fire, how Climate Change Contributes to Recent. Cambridge Press, Catastrophes (in Press).

Funk, C., Peterson, P., Landsfeld, M., Coauthors, 2015. The climate hazards infrared precipitation with stations – a new environmental record for monitoring extremes. Sci. Data 2, 150066. https://doi.org/10.1038/sdata.2015.66.

Gu, G.J., Adler, R.F., 2004. Seasonal evolution and variability associated with the West African monsoon system. J. Clim. 17, 3364–3377.

Harrison, L., Funk, C., Peterson, P., 2019. Identifying changing precipitation extremes in Sub-Saharan Africa with gauge and satellite products. Environ. Res. Lett. 14, 085007.

Hastenrath, S., 2001. Variations of East African climate during the past two centuries. Clim. Chang. 50, 209–217.

Hastenrath, S., 2007. Circulation mechanisms of climate anomalies in East Africa and the equatorial Indian Ocean. Dyn. Atmos. Oceans 43, 25–35.

Hastenrath, S., Polzin, D., Mutai, C., 2011. Circulation mechanisms of Kenya rainfall anomalies. J. Clim. 24, 404–412.

Hersbach, H., et al., 2020. The ERA5 global reanalysis. Quart. J. Roy. Meteor. Soc. 146, 1999–2049.

Hua, W., Zhou, L., Chen, H., Nicholson, S.E., Raghavendra, R., Jian, Y., 2016. Possible causes of central equatorial long-term drought. Environ. Res. Lett. 11, 1234002 https://doi.org/10.1088/1748-9326/1112/124002.

Huffman, G.J., et al., 2020. Integrated multi-satellite retrievals for the global precipitation measurement (GPM) mission (IMERG). In: Satellite Precipitation Measurement. Springer, Cham, pp. 343–353.

Jackson, L.S., Keane, R.J., Finney, D.L., Marsham, J.H., Parker, D.J., Senior, C.A., Stratton, R.A., 2019. Regional differences in the response of rainfall to convectively coupled Kelvin waves over tropical Africa. J. Clim. 32, 8143–8165.

Kimani, M., Hoedjes, J., Su, Z., 2017. An assessment of satellite-derived rainfall products relative to ground observations over East Africa. Remote Sens. 9, 430–450. https://doi.org/10.3390/rs9050430.

Kimani, M., Hoedjes, J., Su, Z., 2018. Bayesian bias correction of satellite rainfall estimates for climate studies. Remote Sens. 10, 1–18. https://doi.org/10.3390/rs9050430.

Klein, C., Nkrumah, F., Taylor, C.M., Adefisan, E.A., 2021. Seasonality and trends of drivers of mesoscale convective systems in Southern West Africa. J. Clim. 34, 71–87. https://doi.org/10.1175/JCLI-D-20-0194.1.

Koros, D., 2020. Weather and Desert Locusts. Report of the Kenya Meteorological Department, p. 18.

Laing, A.G., Carbone, R.E., Levizzani, V., 2011. Cycles and propagation of deep convection over equatorial Africa. Mon. Weather Rev. 139, 2832–2853. https://doi.org/10.1175/2011MWR3500.1.

Lutz, K., Rathman, J., Jacobeit, J., 2013. Classification of warm and cold water events in the eastern tropical Atlantic Ocean. Atmos. Sci. Lett. 14, 102–106.

Lutz, K., Jacobeit, J., Rathmann, J., 2015. Atlantic warm and cold water events and impact on west coast precipitation. Int. J. Climatol. 35, 28–141.

Maranan, M., Fink, A.H., Knippertz, P., 2018. Rainfall types over southern West Africa: Objective identification, climatology and synoptic environment. Quart. J. Roy. Met. Soc. 144, 1628–1648. https://doi.org/10.1002/qj.3345.

Mekonnen, A., 2020. Africa [in State of the climate in 2019″]. Bull. Amer. Meteor. Soc. 101, S350–S362. https://doi.org/10.1175/2020BAMSStateoftheClimate_Chapter7.e.

Monerie, P.-A., Biasutti, M., Roucou, P., 2016. On the projected increase of Sahel rainfall during the late rainy season. Int. J. Climatol. 113, 4373–4383.

Muller, C., Takayab, Y., 2020. Response of precipitation extremes to warming. What have we learned from theory and idealized cloud-resolving simulations, and what remains to be learned? Environ. Res. Lett. 15, 035001.

Nicholson, S.E., 1986a. The spatial coherence of African rainfall anomalies. Interhemispheric teleconnections. J. Climate Appl. Meteor 25, 1365–1381.

Nicholson, S.E., 1986b. The nature of rainfall variability in Africa south of the equator. J. Climatol. 6, 515–530.

Nicholson, S.E., 2014. Spatial teleconnections in African rainfall:a comparison of 19th and 20th century patterns. The Holocene 24, 1840–1848.

Nicholson, S.E., 2015. Long-term variability of the East African "short rains" and its links to large-scale factors. Int. J. Climatol. 35, 3979–3990.
Nicholson, S.E., 2021. The rainfall and convective regime over equatorial Africa, with emphasis on the Congo Basin. In: Alsdorf, D., Tshimanga, R., Moukandi, G. (Eds.), Congo Basin Hydrology, Climate and Biogeochemistry. AGU Monograph, Wiley and Sons in press.
Nicholson, S.E., Entekhabi, D., 1987. Rainfall variability in equatorial and southern Africa: relationships with sea surface temperatures along the southwestern coast of Africa. J. Clim. Appl. Meteorol. 26, 561–578.
Nicholson, S.E., Kim, J., 1997. The relationship of the El-Niño southern oscillation to African rainfall. Int. J. Climatol. 17, 117–135.
Nicholson, S.E., Webster, P.J., 2007. A physical basis for the interannual variability of rainfall in the Sahel. Quart. J. Roy. Meteor. Soc. 133, 2065–2084.
Nicholson, S.E., Fink, A.H., Funk, C., 2018a. Assessing recovery and regime change in West African rainfall from a 161-year record. Int. J. Climatol. 38, 3770–3786.
Nicholson, S.E., Funk, C., Fink, A.H., 2018b. One and a half centuries of rainfall variability over the African continent. Glob. Planet. Chang. 165, 114–127.
Nicholson, S.E., Klotter, D., Zhou, L., Hua, W., 2019. Validation of satellite precipitation estimates over the Congo Basin. J. Hydrometeorol. 20, 631–656.
Okumura, Y., Xie, S.P., 2004. Interaction of the Atlantic equatorial cold tongue and the African monsoon. J. Clim. 17, 3589–3602.
Opoku-Ankomah, Y., Cordery, I., 1994. Atlantic Sea-surface temperatures and rainfall variability in Ghana. J. Clim. 7, 551–558.
Pohl, B., Camberlin, P., 2006. Influence of the Madden–Julian oscillation on East African rainfall. I. Intraseasonal variability and regional dependency. Quart. J. Roy. Meteor. Soc. 132, 2521–2539.
Ratna, S.B., Cherchi, A., Osborn, T.J., Joshi, M., Uppara, U., 2020. The Extreme positive Indian Ocean Dipole of 2019 and Associated Indian Summer Monsoon Rainfall Response. Geophys. Res. Lett. 48 https://doi.org/10.1029/2020GL091497.
Reed, R.J., Norquist, D.C., Recker, E.E., 1977. The structure and properties of African wave disturbances observed during phase III of GATE. Mon. Weather Rev. 105, 317–333.
Ropelewski, C.F., Halpert, M.S., 1987. Global and regional scale precipitation associated with El Nino/Southern Oscillation. Mon. Weather Rev. 115, 985–996.
Sandjon, A.T., Nzeukou, A., Tchawoua, C., Sonfack, B., Siddi, T., 2014. Comparing the patterns of 20–70 days intraseasonal oscillations over Central Africa during the last three decades. Theor. Appl. Climatol. 118, 1–11. https://doi.org/10.1007/s00704-013-1063-1.
Satge, F., Defrance, D., Sultan, B., Bonnet, M.P., Seyler, F., Rouche, N., Pierron, F., Paturel, J.E., 2020. Evaluation of 23 gridded precipitation datasets across West Africa. J. Hydrol. 581 https://doi.org/10.1016/j.jhydrol.2019.124412.
Schlueter, A., Fink, A.H., Knippertz, P., Vogel, P., 2019. A systematic comparison of tropical waves over northern Africa. Part 1: influence on rainfall. J. Clim. 32, 1501–1523. https://doi.org/10.1175/JCLI-D-18-0173.1.
Schreck, C.J., Semazzi, F.H.M., 2004. Variability of the recent climate of eastern Africa. Int. J. Climatol. 24, 681–701.
Schwendike, J., Govekar, P., Reeder, M.J., Wardle, R., Berry, G.J., Jakob, C., 2014. Local partitioning of the overturning circulation in the tropics and the connection to the Hadley and Walker circulations. J. Geophys. Res.-Atmos. 119, 1322–1339.
Sinclaire, Z., Lenouo, A., Tchawoua, C., Janicot, S., 2015. Synoptic Kelvin type perturbation waves over Congo basin over the period 1979-2010. J. Atmos. Sol.-Terr. Phys. 130-131, 43–56.
Skofronick-Jackson, G., et al., 2017. The global precipitation measurement (GPM) mission for science and society. Bull. Amer. Meteor. Soc. 98, 1679–1695.
Slingo, J., Spender, H., Hoskins, B., Berrisford, P., Black, E., 2005. The meteorology of the Western Indian Ocean, and the influence of the east African highlands. Phil. Trans. R. Soc. A 363, 25–42.
Trenberth, K.E., et al., 2003. The changing character of precipitation. Bull. Amer. Meteor. Soc. 84, 1205–1218.
Ummenhofer, C.C., Sen Gupta, A., England, M.H., Reason, C.J.C., 2009. Contributions of Indian Ocean sea surface temperatures to enhanced East African rainfall. J. Clim. 22, 993–2013.
Vallès-Casanova, I., Lee, S.K., Foltz, G.R., Pelegrí, J.L., 2020. On the spatiotemporal diversity of Atlantic Niño and associated rainfall variability over West Africa and South America. Geophys. Res. Lett. 47, e2020GL087108.
van der Linden, R., Fink, A.H., Pinto, J.G., Phan, V.T., Kiladis, G.N., 2016. Modulation of daily rainfall in Southern Vietnam during the Southwest monsoon season by the Madden-Julian oscillation and convectively coupled equatorial waves. J. Clim. 29, 5801–5820. https://doi.org/10.1175/JCLI-D-15-0911.1.
Wagner, R.G., DaSilva, A.M., 1994. Surface conditions associated with anomalous rainfall in the Guinea coastal region. Int. J. Climatol. 14, 179–199.
Wainwright, C.M., Finney, D.L., Kilavi, M., Black, E., Marsham, J.M., 2020. Extreme rainfall in East Africa, October 2019–January 2020 and context under future climate change. Weather 76, 26–30.
Wainwright, C.M., Marsham, J.H., Rowell, D.P., Finney, D.L., Black, E., 2021. Future changes in seasonality in East Africa from regional simulations with explicit and parameterized convection. J. Clim. 34, 1367–1385.
Wang, G., et al., 2020. A unique feature of the 2019 extreme positive Indian Ocean Dipole event. Geophys. Res. Lett. 47, e2020GL088615.
Webster, P.J., Moore, A.M., Loschnigg, J.P., Leben, R.R., 1999. Coupled ocean-atmosphere dynamics in the Indian Ocean during 1997–98. Nature 401, 356–360.
Wheeler, M., Kiladis, G.N., 1999. Convectively coupled equatorial waves. Analysis of clouds and temperature in the wavenumber–frequency domain. J. Atmos. Sci. 56, 374–399. https://doi.org/10.1175/1520-0469(1999)056,0374:CCEWAO.2.0.
Woodruff, S.D., Worley, S.J., Lubker, S.J., Ji, Z.H., Freeman, J.E., Berry, D.I., Brohan, P., Kent, E.C., Reynolds, R.W., Smith, S.R., Wilkinson, C., 2011. ICOADS Release 2.5: extensions and enhancements to the surface marine meteorological archive. Int. J. Climatol. 31, 951–967.